MD Simulations of Acyclic and Macrocyclic Gd^{3+}-Based MRI Contrast Agents: Influence of the Internal Mobility on Water Proton Relaxivity[±]

Fabrice Yerly,[a] Alain Borel,[b] Lothar Helm,[a] and André E. Merbach*[a]

Abstract: Classical molecular dynamics simulations with a force field adapted to the family of Gd^{3+} polyaminocarboxylate complexes have been successfully applied on two macrocyclic ($[Gd(DOTA)(H_2O)]^-$ and $[Gd(DO3A)(H_2O)_2]$) and two acyclic ($[Gd(DTPA)(H_2O)]^{2-}$ and $[Gd(EGTA)(H_2O)]^-$) complexes in aqueous solution (DOTA = 1,4,7,10-tetrakis(carboxymethyl)-1,4,7,10-tetraazacyclododecane, DO3A = 1,4,6-tris(carboxymethyl)-1,4,7,10-tetraazacyclododecane, DTPA = 1,1,4,7,7-pentakis(carboxymethyl)-1,4,7-triazaheptane, EGTA = 1,1,10,10-tetrakis(carboxymethyl)-1,10-diaza-4,7-dioxadecane). In both macrocylic complexes the Gd^{3+} coordination polyhedron remains close to a monocapped square antiprism (MSA) during the entire simulation time. For the stereolabile acyclic complexes different interconverting sets of geometries are observed: three sets close to tricapped trigonal prisms (TTP) for $[Gd(EGTA)(H_2O)]^-$ and three sets intermediate between MSA and TTP (distorted C_{2v} symmetry) for $[Gd(DTPA)(H_2O)]^{2-}$. The fast conformational changes observed in the acyclic complexes might weaken the hydration of the second water shell and therefore disfavour the outer-sphere relaxivity. Moreover, the motions of the chelate observed in both acyclic complexes involve the reorientation of the symmetry elements over time. This reorientation, occurring on a picosecond timescale, can be associated with the correlation time for modulation of the zero field splitting and might participate in the electron spin relaxation mechanisms of the Gd^{3+} ion. The internal motion of the inner-sphere water molecule can be quantified by the ratio τ_R(GD–HW)/τ_R(GD–OW) which increases slightly from 0.7 for the acyclic to 0.8 for the macrocyclic complexes. This increase for the macrocylic chelates is favourable for a higher relaxivity and can be related to their rigidity. The water exchange rate on the four complexes has been related to the steric constraint of the ligand on the inner-sphere water molecule(s), which is inversely proportional to a geometrical descriptor, the solid angle ψ. A range of ψ values is given ($2 \ll \psi < 3.3$) where the exchange should be optimal. The observations made on the picosecond timescale give general directions for the design of more efficient magnetic resonance imaging contrast agents.

Keywords: conformation analysis · gadolinium · hydration effects molecular dynamics · MRI contrast agents

Introduction

In the last two decades, magnetic resonance imaging (MRI) has become more and more popular as a medical method of diagnosis. The use of contrast agents that increase the relaxation rates of the water protons has considerably improved the quality of the imaging.[1–3] Most of these contrast agents are complexes of the highly paramagnetic Gd^{3+} ion (S = 7/2). As $[Gd(H_2O)_8]^{3+}$ is toxic when administrated directly into the body, inert and stable Gd^{3+} complexes are used to take advantage of the magnetic properties of the metal ion without incurring its undesirable effects. The stability of the medical Gd^{3+} complexes has to match severe criteria, verified by competitive potentiometry.[4,5] The architecture of the ligands has a strong influence on the efficiency—-that is, the relaxivity—of the complexes in solution. From theoretical considerations one knows that complexes that are inject-

[a] Prof. A. E. Merbach, F. Yerly, Dr. L. Helm
Institut de Chimie Moléculaire et Biologique
Ecole Polytechnique Fédérale de Lausanne
1015 Lausanne (Switzerland)
Fax: (+41) 216-939-875
E-mail: andre.merbach@epfl.ch

[b] Dr. A. Borel
Illinois EPR Research Center and Department of Chemistry
University of Illinois
Urbana (USA)
Fax: (+1) 217-333-8868
E-mail: aborel@uiuc.edu

[+] MD = molecular dynamics, MRI = magnetic resonance imaging.

Supporting information for this article is available on the WWW under http://www.chemeurj.org/ or from the author.

© 2003 Wiley-VCH Verlag GmbH & Co. KGaA, Weinheim
DOI: 10.1002/chem.200305175

ed today for medical imaging are far away from a maximum possible relaxivity.[1]

A rational approach to finding better contrast agents is to determine all the parameters that govern the relaxivity of existing complexes and to derive structure–activity relationships. It has been shown that a longer rotational correlation time of the inner-sphere water protons combined with an increase of the water exchange rate compared to those of the presently used contrast agents such as $[Gd(DOTA)(H_2O)]^-$ could considerably increase the proton relaxivity. Increasing the rotational correlation time has been achieved by synthetic chemists, who built larger molecules of either covalently attached complexes, for example, dendrimers,[6] or noncovalently bound interacting systems, for example, micellar or protein complexes. Despite the efforts made to increase the water exchange rate on the paramagnetic centre, there are today very few Gd^{3+} complexes that have both an optimal water exchange rate and a sufficient stability and inertness in a biological medium, and they are still not used in medicine.[7–9]

The determination of the parameters involved in the relaxivity is best achieved by fitting globally the data obtained for each contrast agent by ^{17}O NMR, NMRD and EPR spectroscopies with an ad hoc theoretical model.[10] This approach increases the number of constraints on the fit and allows a greater confidence in the obtained parameters than for separate analysis. Further recent refinements of the theoretical model lead to a better understanding of the physical meaning of the fitted parameters. For example, a physically more accurate description of the electron spin relaxation[11–13] has been introduced in the global fitting procedure.[14] Other experimental techniques were also used to obtain complementary information of the solution behaviour of contrast agents. For example, replacing the Gd^{3+} ion by an Eu^{3+} ion allows multinuclear NMR studies to determine the complex structures in solution,[15–17] UV/Vis spectroscopy to study hydration equilibriums of the metal ions[18–20] or luminescence experiments to measure lifetimes and populations of the water molecules in the first shell of lanthanide ions.[21]

Alongside the experimental studies, computational chemistry is a unique tool to get information at the molecular level in solution. For instance Cosentino et al.[22] have studied various lanthanide(III) complexes with $DOTA^{4-}$ by ab initio methods in vacuo. They were able to calculate the conformational energies of various isomeric forms plus the interconversion pathways and corresponding energy profiles. Classical molecular dynamics (MD) simulations were performed on Ln^{3+} complexes with $DOTA^{4-}$ to reproduce the molecular structures and stabilities of the major and minor isomers in aqueous solution.[23] Bonds were imposed between the Ln^{3+} ion and the coordination sites to lend stability to the complexes and to maintain them stable in solution; this of course forbids a study of the internal mobility. Another classical MD simulation study has been performed on various MRI-relevant Gd^{3+} chelates by Borel et al.[24] In the latter study the structures of the complexes were frozen to prevent dissociation of the complex, with the goal being to study their hydration to calculate the outer-sphere relaxivity. The recent development of a force field that enables to reproduce also the intramolecular behaviour of a Gd^{3+} complex in aqueous solution by MD simulation[25] has opened a new way to investigate the domain of MRI contrast agents, since it gives information at the molecular level and the picosecond time scale on internal motions that are involved in the relaxivity process. In fact the rotational/translational diffusion of the complex, the water exchange rate on the Gd^{3+} ion and its electron spin relaxation, which are the three main factors affecting the relaxivity, are related to the internal motions of the contrast agents.

In this study we wish to characterise the molecular mobility of various Gd^{3+} chelates in order to link the motions observed through MD simulations with their relaxivities. A

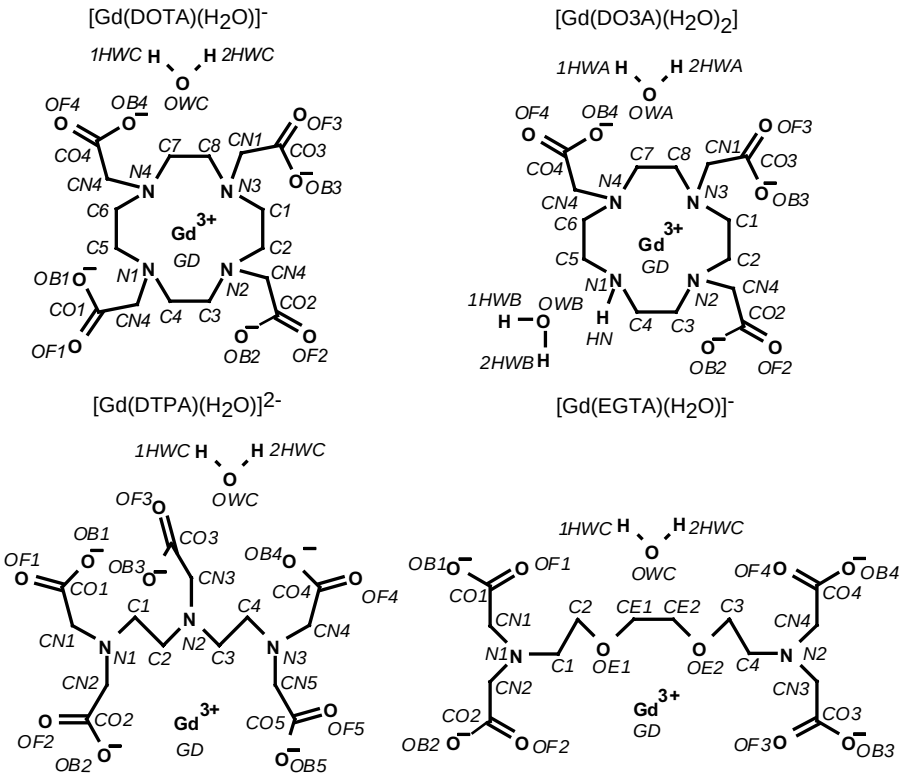

Scheme 1. Schematic diagrams of the studied complexes indicating the structure of the ligands and the atom names. DOTA = 1,4,7,10-tetrakis(carboxymethyl)-1,4,7,10-tetraazacyclododecane, DO3A = 1,4,6-tris(carboxymethyl)-1,4,7,10-tetraazacyclododecane, DTPA = 1,1,4,7,7-pentakis(carboxymethyl)-1,4,7-triazaheptane, EGTA = 1,1,10,10-tetrakis(carboxymethyl)-1,10-diaza-4,7-dioxadecane.

 © 2003 Wiley-VCH Verlag GmbH & Co. KGaA, Weinheim

popular class of ligands are polyaminocarboxylates, which can be either macrocyclic, for example, $DOTA^{4-}$ and $DO3A^{3-}$, or acyclic like $DTPA^{5-}$ or $EGTA^{4-}$ (Scheme 1). The $[Gd(DOTA)(H_2O)]^-$ and $[Gd(DTPA)(H_2O)]^{2-}$ complexes are currently used for medical applications. The relatively high water exchange rate of $[Gd(EGTA)(H_2O)]^-$ and the higher hydration number of $[Gd(DO3A)(H_2O)_2]$ make them good models for the comprehension of the parameters of prospective contrast agents. The picosecond resolution, combined with the versatility of the new force field, makes classical MD simulation an attractive tool for the understanding of the more obscure properties of the contrast agents, such as the Gd^{3+} electronic spin relaxation and the internal motion of the water molecules bound to the metal ion.

Results and Discussion

Solution structure of the chelates: The complexation of the Gd^{3+} ion is described by a pure nonbonding interaction in our classical MD simulations. It means that the coordinated nitrogen atoms, the water and the carboxylate oxygen atoms can, in principle, leave the metal coordination sphere because they are not attached by an artificial constraint. The MD simulation timescale is shorter than the experimental water residence time in the first shell, τ_M, by at least one order of magnitude for the fastest exchanging complex, $[Gd(EGTA)(H_2O)]^-$. Experimental water exchange rates for the various complexes are between 3.3×10^6 and $31\times10^6\ s^{-1}$.[1] Nevertheless some events involving the departure, the arrival and the exchange of water molecules were observed in the MD simulations. In the $[Gd(EGTA)(H_2O)]^-$ simulation,[25] the inner-sphere water molecule left the complex and was not replaced. This was explained by the inability of our model to describe the gradual polarisation of the water molecules when approaching the complex. The duration of this water molecule in the coordinated state was long enough (about 500 ps) to study the behaviour in solution of the hydrated complex $[Gd(EGTA)(H_2O)]^-$. In the $[Gd(DTPA)(H_2O)]^{2-}$ simulation, the inner-sphere water molecule left the complex at 832 ps, going to a distance of 3.7 Å from the Gd^{3+} ion. After the departure of this water molecule, its polarisation was removed and normal TIP3P charges were assigned. This water molecule stayed out of the first shell for a very short time (0.4 ps), then came back and was repolarised. In the $[Gd(DO3A)(H_2O)_2]$ simulation, both inner-sphere water molecules stayed in the inner sphere during the whole simulation time (1000 ps). In solution the complex $[Gd(DOTA)(H_2O)]^-$ exists as two stereoisomers in equilibrium, the so-called major M (about 80%) and minor m (about 20%) isomers.[26] In this paper we present a simulation of the M isomer of the Gd^{3+} complex, for which there are crystallographic data. We tried to perform a simulation of the minor m isomer by starting from X-ray data of $[La(DOTA)(H_2O)]^-$.[27] Unfortunately we did not succeed in obtaining a stable complex in solution. With the M isomer of $[Gd(DOTA)(H_2O)]^-$, one water exchange was observed: at 137.6 ps, the inner-sphere water molecule left the complex and immediately moved farther than 7 Å from the Gd^{3+} ion. At 159.4 ps, another water molecule entered the inner sphere, replacing the first one, and was then repolarised. Although there should be no water departure or incoming events during the 1 ns MD simulations on the Gd^{3+} ions, a few not statistically relevant events were observed. One possible cause is that we used a static atomic charge model with no dynamic polarisation of the donor atoms.

Selected mean distances of the complexes measured in the MD simulations and in the X-ray solid-state molecular structures are presented in Table 1. GD–OB distances are generally longer in MD simulations than in the solid state by about 5%, except for the $DOTA^{4-}$ complex where this distance is 7% shorter. GD–N distances are shorter in MD simulations than in the solid state by approximately 2–4%, except for the $EGTA^{4-}$ complex where this distance is 2% longer. GD–OWC distances are greater in MD simulations than in the solid state by about 2–5%. This can be explained by the interaction of the inner-sphere water protons with the bulk through the formation of hydrogen bonds with the water oxygens of the second shell. This hydrogen-bond formation might be more important here than was observed by Borel et al.[24] due to the greater polarisation of the inner-sphere water molecule in the new charge model (−1.05 and +0.525 for OWC and HWC, respectively). The $DOTA^{4-}$ and the $DO3A^{3-}$ complexes show very similar distances between the metal ion and coordinated atoms. The only significant difference, observed in the solid state, is the shorter GD–OB distance in the $DO3A^{3-}$ complex. Nevertheless, the distances measured in simulated solution are close to the corresponding distances in the solid state: the difference is always less than the standard deviation calculated for the MD simulations.

Table 1. Selected mean distances [Å] measured from the MD simulations (MDS) and from the X-ray solid-state structures (XR) of the various Gd^{3+} complexes. Standard deviations are given in brackets.

Distance	$DOTA^{4-}$		$DO3A^{3-}$		$DTPA^{5-}$		$EGTA^{4-}$[25]	
	MDS	XR	MDS	XR	MDS	XR	MDS	XR
GD–OB	2.48(6)	2.66	2.48(6)	2.35	2.53(8)	2.39	2.50(7)	2.36
GD–OF	4.44(12)	4.44	4.46(11)	4.44	4.47(13)	4.41	4.45(12)	4.37
GD–N	2.61(6)	2.66	2.61(6)	2.68	2.58(6)	2.68	2.59(7)	2.53
GD–OE	–	–	–	–	–	–	2.46(6)	2.52
GD–OWC	2.59(9)	2.46	2.58(8)[a]	–	2.59(8)	2.44	2.59(8)	2.53
GD–HWC	3.27(13)	2.94	3.26(14)[a]	–	3.25(14)	–	3.26(19)	–

[a] The $DO3A^{3-}$ complex has two inner-sphere water molecules, A and B. Here the letter C (OWC, HWC) is used as an averaged value between A and B.

The dihedral angles that link the coordinated atoms of the various complexes describe the complete stereochemical conformation of the complex. The $[Gd(EGTA)(H_2O)]^-$ simulations showed a high stereolability of the complex, with fast conformational changes of the ligand during the simula-

© 2003 Wiley-VCH Verlag GmbH & Co. KGaA, Weinheim

tion.[25] We present in Figure 1 the time evolution of the dihedral angles of $[Gd(DOTA)(H_2O)]^-$ and $[Gd(DTPA)(H_2O)]^{2-}$. Dihedral angles of $[Gd(DO3A)(H_2O)_2]$ are not shown here since they are very close to the $DOTA^{4-}$ complex (see Supporting Information). For both macrocyclic complexes, the structure of the ligand remains highly rigid during the whole simulation. No conformation changes are observed, and the values in solution stay close to the solid-state ones. In the various complexes there are two types of dihedral angles. N–C–C–OB acetate dihedral angles have one bridging carbon atom (CH_2) that has a tetrahedral sp^3 environment and another carbon atom (CO) that has a trigonal sp^2 environment. This leads to dihedral angles for these acetate groups that are around $\pm 30°$. All the other dihedral angles (N–C–C–N and N–C–C–OE angles, see Scheme 1) have two bridging carbon atoms that are tetragonal sp^3, which leads to greater angles of about $\pm 60°$. The interconversion energy for the acetate dihedral angles is consequently lower than that for the other angles. This is clearly shown in Figure 1: for $[Gd(DTPA)(H_2O)]^{2-}$, the two N–C–C–N dihedral angles remain in a $\lambda\lambda$ conformation (value around $-60°$) during the whole 1 ns simulation whereas the acetate dihedral angles (N–C–C–OB) change their conformation. They flip so fast from positive to negative values that it is not possible to define periods where the ligand has an accurate, well-defined conformation.

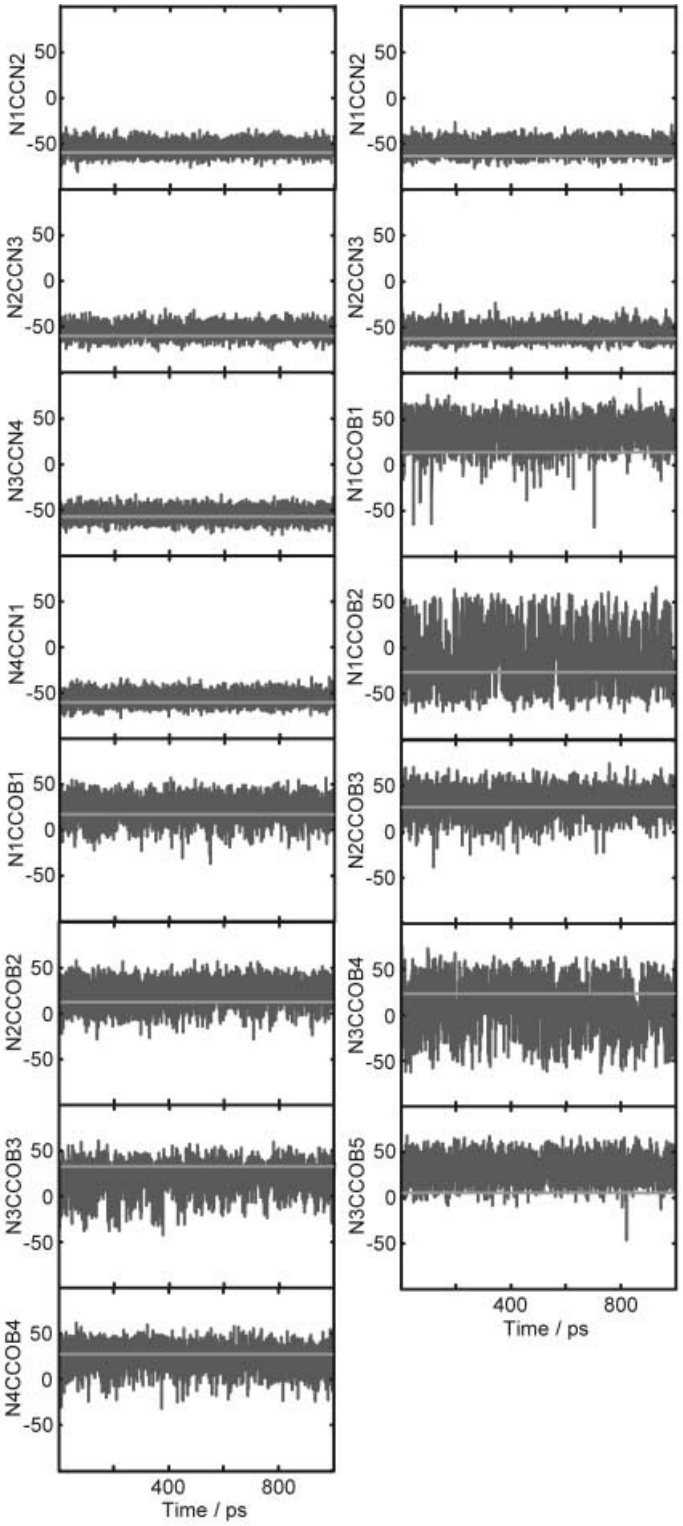

Figure 1. Time evolution of the dihedral angles of $[Gd(DOTA)(H_2O)]^-$ (left) and $[Gd(DTPA)(H_2O)]^{2-}$ (right). Atom labels refer to Scheme 1. The light grey line = the corresponding angle in the solid state.

In conclusion the distances between the complex atoms observed in simulated solutions are similar to the ones observed in the solid state. The macrocyclic complexes $[Gd(DOTA)(H_2O)]^-$ and $[Gd(DO3A)(H_2O)_2]$ are highly rigid, keeping their solution conformation close to the solid-state one during the whole 1 ns simulations. For these complexes only small oscillations of the dihedral angles around the X-ray data values have been observed. On the other hand the acyclic complexes $[Gd(EGTA)(H_2O)]^-$ and $[Gd(DTPA)(H_2O)]^{2-}$ change their conformation during the simulation. However the solid-state structures we used as the initial structures also exist in the simulated solutions. For these complexes the averaged structure of all the conformations observed in simulated solution is not equal to the solid-state structure.

Description of the solvation of the Gd^{3+} chelates: The proton relaxivity of a Gd^{3+} complex, which describes the efficiency of the complex as a potential MRI contrast agent, is commonly divided into inner-sphere, r_{is}, and outer-sphere, r_{os}, contributions.[1] The outer-sphere relaxivity is mainly due to the distribution and the dynamic behaviour of the bulk water molecules in the vicinity of the complex. By using the radial distribution functions of the water protons around the paramagnetic centre and a suitable model of the electron spin relaxation it is possible to calculate r_{os}. This was performed in an earlier paper on various complexes, including $[Gd(DOTA)(H_2O)]^-$ and $[Gd(DTPA)(H_2O)]^{2-}$, by using a force field tailored to reproduce an ad hoc external electrostatic potential of each complex with charges calculated with the Merz–Kollman (MZK) model.[24] In this previous force field, the choice of the atomic charges, optimised to reproduce an external electrostatic potential, led to poor complex stability, which was compensated for by the use of a frozen molecular structure of the complexes. The new force field used in the present work leads to a stable complex in solution and does not require a frozen structure. However, the atomic charges of the complexes, calculated by the Mulliken method (MUL), are not optimised to describe the ex-

 © 2003 Wiley-VCH Verlag GmbH & Co. KGaA, Weinheim

ternal potential energy, like the previous ones, but rather to reproduce the coordination structure and dynamics of the Gd^{3+} centre in solution. We wish to compare the changes in the radial distribution functions (*rdf*s) and outer-sphere relaxivities resulting from both force fields (Figure 2).

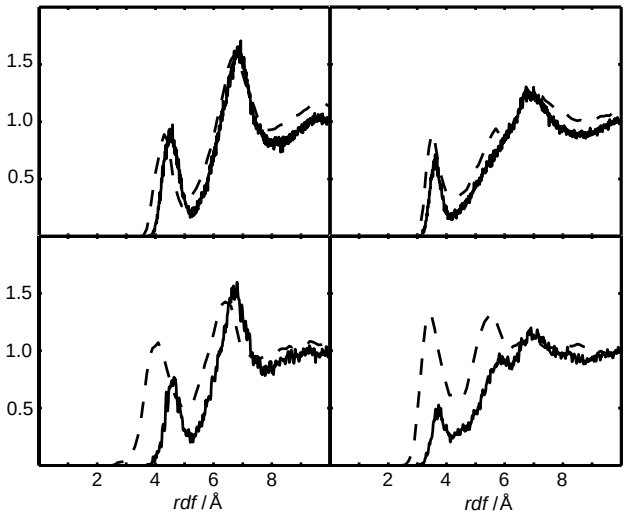

Figure 2. Radial distribution functions *rdf* around the Gd^{3+} ion in $[Gd(DOTA)(H_2O)]^-$ (top) and $[Gd(DTPA)(H_2O)]^{2-}$ (bottom) of the outer-sphere water oxygen (left) and hydrogen (right) atoms from simulations with the previous force field MZK (dashed lines) and the new force field MUL (solid lines).

Radial distribution functions calculated on the rigid $[Gd(DOTA)(H_2O)]^-$ are close for both force fields. In the new MUL force field the second-shell peaks of the water hydrogen and oxygen atoms are only 0.15 Å farther away from the metal ion. The complex $[Gd(DTPA)(H_2O)]^{2-}$ gives clearly different *rdf*s depending on the model used. The second-shell water oxygen and hydrogen peaks are significantly farther away and smaller in the new force field. There are two possible reasons that explain this difference. The first one is that the atomic charges are different for the old MZK and the new MUL force fields and this leads to a different external electrostatic potential, which is, in principle, better described by the MZK force field. The second reason is that the higher mobility of the $DTPA^{5-}$ complex, observed only by the new MUL force field, can affect the second hydration sphere. The latter reason would also explain why the *rdf*s obtained from both force fields are close for the $DOTA^{4-}$ complex, since the frozen structure MZK force field is more realistic in this case than for the acyclic mobile complexes.

Consequently, the calculated $[Gd(DOTA)(H_2O)]^-$ outer-sphere relaxivity is slightly lower (by 0.2–0.8 $mM^{-1}\,s^{-1}$ depending on the magnetic field) for the new MUL force field due to the 0.15 Å increase in distance of the water second shell (see Supporting Information). The difference is more important (0.5–1.4 $mM^{-1}\,s^{-1}$ lower in the MUL force field) for $[Gd(DTPA)(H_2O)]^{2-}$ due to the lower hydration number and the increase in the distance between the Gd^{3+} ion and the water second shell. Incidentally, replacing the empirical electron spin relaxation equations of Powell et al.[10] by a more rigorous description[10–14,28,29] has no significant influence on the calculated outer-sphere relaxivity for these complexes with either the MUL or MZK force fields. For complexes $[Gd(DOTA)(H_2O)]^-$ and $[Gd(DTPA)(H_2O)]^{2-}$ there is no direct experimental data on r_{os} because the measured relaxivity profile is the sum of the inner- and outer-sphere contributions. For a small complex with one water molecule in the inner sphere, r_{os} represents about half of the overall relaxivity. In order to check if the internal mobility of the complex really has an influence on the outer-sphere relaxivity, as we can suppose from the comparison between both force fields, one should compare the experimental/computational studies of Gd^{3+} complexes with no water molecule in the inner sphere. This would give a direct experimental access to the outer-sphere relaxivity. By studying rigid and mobile complexes and comparing *rdf* results for both MKZ and MUL force fields, it would be possible to confirm that a higher internal mobility of a complex tends to decrease its outer-sphere relaxivity.

Symmetry analysis: The algorithm developed in a previous paper[25] to find the best tricapped trigonal prism (TTP) of symmetry D_{3h} and the best monocapped square antiprism (MSA) of symmetry C_{4v} for a given coordination polyhedron has been applied to the various MD simulations. For each 0.2 ps recorded time step, we searched for the best TTP and the best MSA. The resulting coordination polyhedrons collected over the simulation time steps can be classified into sets of similar geometries that are the closest to an idealised polyhedron that represents the set. To decide if a given polyhedron is closer to a TTP or to an MSA, one needs geometrical descriptors. We have chosen to use the description of Kepert through the angles ϕ_B, ϕ_F, ϕ_C and θ_C (Figure 3).[30]

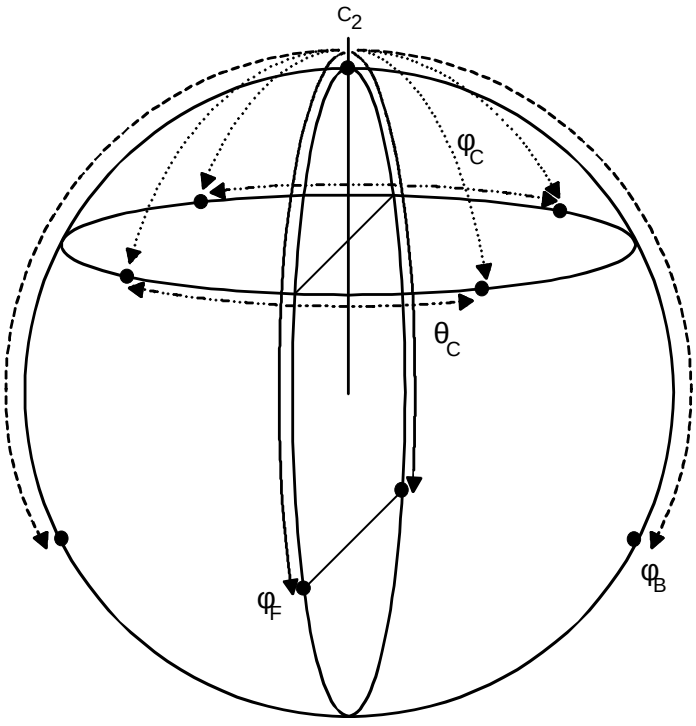

Figure 3. Definition of the angles ϕ_B, ϕ_F, ϕ_C and θ_c by Kepert.[30]

© 2003 Wiley-VCH Verlag GmbH & Co. KGaA, Weinheim

The interconversion energy barrier between the TTP and the MSA is low. The pathway for this interconversion is described by the difference between two angles ϕ_B and ϕ_F. When $|\phi_B-\phi_F|\approx 0°$ the polyhedron is close to an MSA. When $|\phi_B-\phi_F|\approx 14.7°$ the polyhedron is close to a TTP.

In order to determine how close the idealised TTP and/or MSA are to the simulated coordination polyhedrons, we have calculated the angles of interest, by using the idealised polyhedrons found by our algorithm, at each simulation time step. The time-averaged angles calculated on the various idealised polyhedrons are reported in Table 2. Both polyhedrons of the macrocyclic complexes $[Gd(DOTA)(H_2O)]^-$ and $[Gd(DO3A)(H_2O)_2]$ have values that are very characteristic of a C_{4v} symmetry, with a θ_C value that is close to 45° and equal values for ϕ_B and ϕ_F. The polyhedrons of the complex $[Gd(EGTA)(H_2O)]^-$ have angles that are characteristic of a D_{3h} symmetry, with different values for ϕ_B and ϕ_F, close to the theoretical values of 134° and 120° for a TTP,and a θ_C value that is close to 40°. The polyhedrons of the complex $[Gd(DTPA)(H_2O)]^{2-}$ have angle values that are in between, that is, characteristic of an intermediate C_{2v} symmetry, which can be seen either as a distorted MSA or as a distorted TTP.

Table 2. Time-averaged angles calculated for the various idealised polyhedrons found for each Gd^{3+} complex of $DOTA^{4-}$, $DO3A^{3-}$, $DTPA^{5-}$ and $EGTA^{4-}$.

Ligand	Polyhedron	ϕ_A [°]	ϕ_B [°]	ϕ_F [°]	ϕ_C [°]	θ_C [°]
$DOTA^{4-}$	S_1	44.4	125.1	125.1	68.0	44.8
$DO3A^{3-}$	S_1	44.6	125.1	125.5	67.2	45.1
$DTPA^{5-}$	S_1–S_4	44.2	127.3	121.1	68.5	44.2
	S_2–S_4	44.6	129.9	122.7	70.2	46.9
	S_3–S_4	44.8	133.7	124.5	68.9	46.8
$EGTA^{4-}$	S_1	45.6	133.2	121.7	68.2	39.3
	S_2	45.7	136.5	117.6	68.5	40.1
	S_3	44.0	137.5	119.3	68.6	38.3
MSA (Kepert)			127.0	127.0	68.9	45.0
TTP (Kepert)		44.7	134.7	120.0	69.4	40.6

The various coordination polyhedron sets for the four simulated complexes are presented in Figure 4. For each macrocyclic complex $[Gd(DOTA)(H_2O)]^-$ and $[Gd(DO3A)(H_2O)_2]$ one single and unique set is observed during the whole simulation. For both complexes the observed set is an MSA that has its C_4 rotation axis perpendicular to the plane defined by the four nitrogen atoms of the cyclen and the capping position is occupied by a water oxygen atom. The only difference in the $DO3A^{3-}$ complex is that one carboxylate oxygen atom is replaced by the second water oxygen atom.

For the acyclic complexes $[Gd(EGTA)(H_2O)]^-$ and $[Gd(DTPA)(H_2O)]^{2-}$ there are several sets observed during the simulations. In the $EGTA^{4-}$ complex,[25] three sets of TTP polyhedrons were observed. Set S1 has two nitrogen atoms and the inner-sphere water oxygen atom in the capping positions. Sets S2 and S3 have one nitrogen atom, one binding carboxylate oxygen atom and one ether oxygen atom in the capping positions. Looking at the angles of Kepert we remark that the $DTPA^{5-}$ coordination polyhedron is neither an MSA nor a TTP, it is somewhere in between. We nevertheless tried to find the best MSA and TTP polyhedrons. We obtained only three different MSA polyhedrons, called S1, S2 and S3, amongst the many that are theoretically possible. They have the OWC (S1), N3 (S2) and N1 (S3) atoms in their capping positions and represent 73, 17 and 10%, respectively, of the simulation time steps. We also obtained only three different TTP polyhedrons, called S4, S5 and S6. The TTP S4, occupying 87% of the simulation time steps, has the two nitrogen atoms N1 and N3 and the inner-sphere water oxygen atom OWC in the capping positions. TTP S5 and TTP S6 only appear during 11.7 and 1.3%, respectively, of the simulation.

From the three identified TTP polyhedrons of $[Gd(DTPA)(H_2O)]^{2-}$, the polyhedron S4 (see Figure 4) is observed most frequently (87%) and is consistent with the isomeric forms observed by Lammers et al. for various $DTPA^{5-}$-like analogues, [Ln(DTPA-bis(amide))] complexes.[31] The three C_2 axes in TTP S4 are coincident with the C_4 axis of the three observed MSA polyhedrons. This means that the coordination polyhedron of $[Gd(DTPA)(H_2O)]^{2-}$ exists in three different sets that are in between TTP S4 and the three MSAs S1, S2 and S3, as shown in Figure 5. For each set we calculated the distribution of the geometries between the TTP and each of the three MSAs. The difference in angles $|\phi_B-\phi_F|$ is converted here into a percentage of TTP. When the polyhedron is a pure TTP, the value is 100. When it is a pure MSA, the value is 0. A few times in the simulation $|\phi_B-\phi_F|$ is greater than the theoretical value of 14.7° for TTP[30] and, therefore, the distribution contains a few elements above 100%. The S1–S4 set (observed 73% of the simulation time) has a stronger MSA character (43.5% of TTP). The S2–S4 set (17%) is in an intermediate geometry between MSA and TTP (48.2% of TTP). The S3–S4 set (10%) has a stronger TTP character (63.9% of TTP). The two MSAs S2 and S3 are enantiomers when considering only the coordination polyhedron. However, when considering the overall complex, that is, the coordination polyhedron plus the ligand atoms, S2 and S3 are no longer enantiomers. To obtain the mirror image of the these two limiting MSA geometries one needs to change the conformation of the dihedral angles that link the coordination sites of the ligand. In Figure 1, where these angles are represented as a function of time, one notices that during the whole MD simulation the dihedral angles N1–C–C–N2 and N2–C–C–N3 remain in a $\lambda\lambda$ conformation, which is the same conformation as the X-ray crystal structure used as a start for the simulation. During the 1 ns simulation time there is no energy-demanding enantiomerisation of the chiral S1–S4, S2–S4 or S3–S4 sets.

The pathway used by the complex to go from one polyhedron to the other is not obvious, since the trajectory is recorded every 0.2 ps and this leads to a discontinuous trajec-

 © 2003 Wiley-VCH Verlag GmbH & Co. KGaA, Weinheim

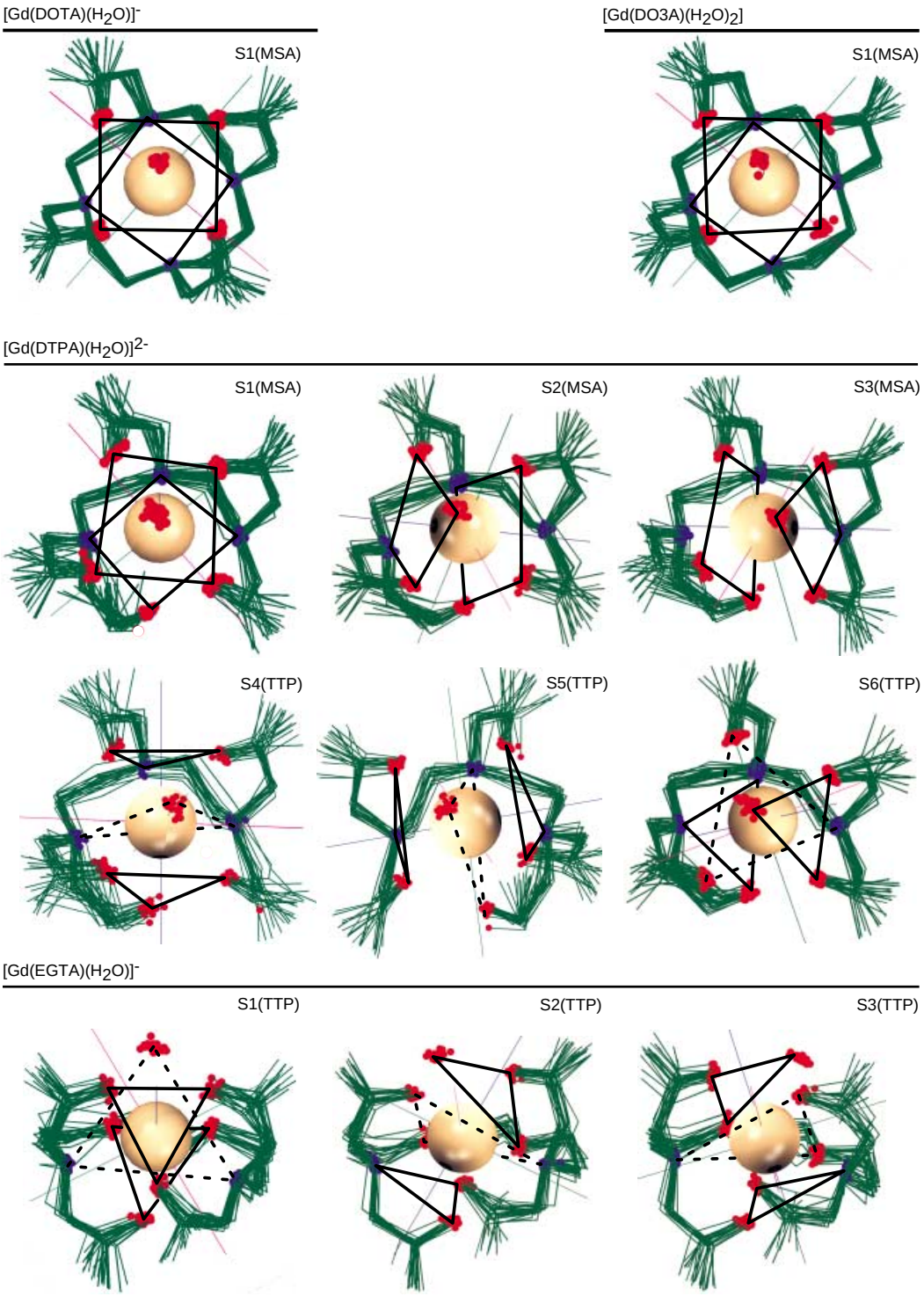

Figure 4. Identified symmetry polyhedrons on the various complexes. Green = ligand, red = oxygen atoms, blue = nitrogen atoms. The black lines show the planes that are othogonal to the main rotational axis (two squares for the MSA and three triangles for the TTP).

tory. Nevertheless we can make some assumptions based on physical considerations. A likely intermediate for all the transformations between the three sets is TTP S4. In fact this TTP has three C_2 rotation axes coincident to the three C_4 axes corresponding to the limiting MSAs S1, S2 and S3. This allows the system to follow a continuous distortion from any of the three sets to the S4 TTP, then again a distortion from this TTP to any other set. This hypothesis is confirmed by the average of the percentage of TTP when the complexes leave or enter into a set. These values are 61.5, 61.1 and 68.1 % of TTP for the sets S1–S4, S2–S4 and S3–S4, respectively, which is always higher than the averaged values for the whole simulation. In S2 the water oxygen atom (OWC) is closer to N1 than to N3 (Scheme 1). In S3

© 2003 Wiley-VCH Verlag GmbH & Co. KGaA, Weinheim

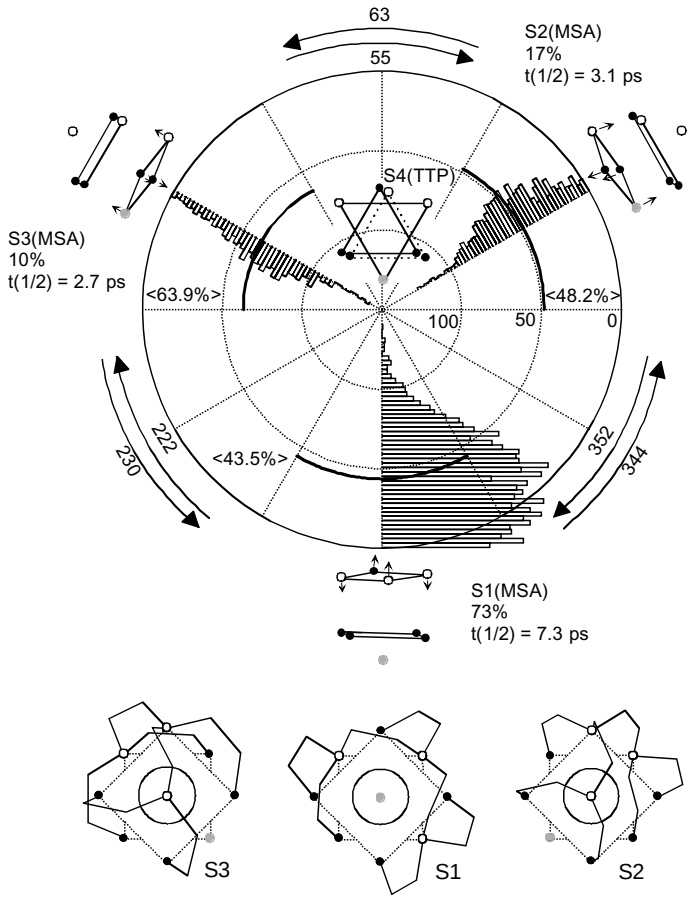

Figure 5. Relationships and pathways between the various identified symmetries in $[Gd(DTPA)(H_2O)]^{2-}$. Labels S1, S2, S3 and S4 refer to Figure 4. The three histograms show the distribution of the polyhedrons in between the pure MSA (0) and the pure TTP (100). Empty circles = nitrogen atoms, black circles = carboxylate oxygen atoms, grey circles = water oxygen atoms. Numbers close to the arrows represent the number of interconversions observed during the simulation. Bottom: the three MSA polyhedrons viewed from the C_4 direction, with the connectivity between the coordination sites.

the reverse is observed: OWC is closer to N3 than N1. By passing from S2–S4 to S3–S4 the OWC will be the same distance from N1 and N3. This equidistance (OWC–N1 equal to OWC–N3) is observed in both S4 and S1 polyhedrons. Thus the S1–S4 set is on the pathway of S2–S4 to S3–S4. This is furthermore confirmed by the higher number of interconversions between the S1–S4 set and either the S2–S4 or S3–S4 sets: both are about five times faster than the S2–S4 to S3–S4 interconversion.

For both acyclic complexes, where the coordination polyhedrons change significantly over the time, one can calculate a lifetime $\tau(S)$ that defines the statistical duration where the polyhedron stays in one set without any change. The mean lifetime τ(mean) is calculated from a weighted average of all the residence correlation functions. Since the crystal field of the ligand can slightly affect the 4f electrons at the quantum level, it is useful to compare the calculated lifetimes with correlation times obtained by experimental methods sensitive to this crystal field. For example, vibrational/collisional modulation of the crystal field splitting is recognised as one contribution to the electron spin relaxation of Gd^{3+} complexes in solution.[11,12] According to recent developments of the theoretical analysis of multiple-temperature and -frequency electron paramagnetic resonance (EPR) data,[13] the correlation time for such a modulation should be on the picosecond timescale. The various lifetimes, and the transient zero field splitting (ZFS) modulation correlation time, τ_V, are reported in Table 3. The lifetime obtained

Table 3. Lifetimes of the various sets of TTP observed for the acyclic Gd^{3+} complexes during the simulations and τ_V.

	Lifetime [ps]	
	$DTPA^{5-}$ TTP–MSA	$EGTA^{4-}$ TTP
τ(S4–S1)	3.1	
τ(S4–S2)	7.3	
τ(S4–S3)	2.7	
τ(S1)		0.69
τ(S2)		6.91
τ(S3)		4.42
τ(mean)	7.2	6.78
τ_V[13]	1.33	

for the $DTPA^{5-}$ complex, of 7.2 ps, is fairly close to the τ_V value of 1.33 ps obtained by Rast et al.[13] The value of 6.78 ps obtained for the $EGTA^{4-}$ complex cannot be compared to an experimentally obtained τ_V in the definition of Rast et al. due to insufficient experimental data. Nevertheless, the nonharmonic fluctuations of the coordination polyhedron of the acyclic complexes can be proposed as one mechanism for the electronic spin relaxation of the Gd^{3+} ion. However in the case of the $DOTA^{4-}$ and the $DO3A^{3-}$ complexes only small vibrations around the MSA symmetry are observed. In fact Rast et al.[11] found values for τ_V in $[Gd(DOTA)(H_2O)]^-$ of about 0.5 ps, which is three times faster than the τ_V value of $[Gd(DTPA)(H_2O)]^{2-}$.

Rotational and translational diffusion: A parameter that strongly influences the water proton relaxivity is the second-order rotational correlation time of the Gd–water proton vector.[2] In a previous paper,[25] we used an MD simulation of $[Gd(EGTA)(H_2O)]^-$ in order to compare different rotational correlation times for this complex. This was done by calculating the rotational correlation times τ_R(Gd–HW), which describes the tumbling of the Gd–HWC vectors (inner-sphere water protons, that is, the correlation time of interest for the relaxivity) and is relevant for the NMRD spectroscopy, τ_R(Gd–OW), which is the slower tumbling time of the Gd–OWC vector (inner-sphere water oxygen atoms) and is relevant for the ^{17}O NMR spectroscopy, and the overall coordination polyhedron rotational correlation time τ_R(polyhedron), which is relevant for the EPR spectroscopy. The same calculation was performed on the simulations of the $DOTA^{4-}$, $DO3A^{3-}$ and $DTPA^{5-}$ complexes (Table 4).

Experimentally τ_R is obtained from the relaxation times of the water oxygen atom and protons and from the Gd^{3+} electronic spin obtained by ^{17}O NMR, NMRD and EPR spectroscopy after a global data analysis.[10] Until recently a single value for τ_R(Gd–HW), τ_R(Gd–OW) and τ_R(polyhe-

 © 2003 Wiley-VCH Verlag GmbH & Co. KGaA, Weinheim

Table 4. Calculated second-order rotational correlation times of the studied Gd^{3+} complexes.

	$DOTA^{4-}$	$DO3A^{3-}$	$DTPA^{5-}$	$EGTA^{4-}$
τ_R(polyhedron) [ps]	52	37	50	43
τ_R(Gd–OW) [ps]	51	36, 33	45	41
τ_R(Gd–HW) [ps]	41	27	32	31
τ_R(expl) [ps]	77[10]	66[32]	58[10]	58[33]
τ_R(HW)/τ_R(OW)	0.82	0.82	0.64	0.72
τ_R(HW)/τ_R(polyhedron)	0.79	0.79	0.70	0.75
τ_R(H_2O) [ps]	1.5	1.3	1.9	1.3

dron) was used in the global data analysis. Since a previous study on the $EGTA^{4-}$ complex introduced discrimination between various τ_R values, we have now to compare rotational correlation times for various vectors with a single experimental value. By convention we will compare τ_R(experimental) with τ_R(polyhedron).

The agreement between the calculated and previously published experimental values for τ_R is reasonable, with differences of approximately 15–30% for the acyclic complexes and of about 38–57% for the macrocyclic complexes. The highest difference occurs for the $DO3A^{3-}$ complex (57%), where the calculated value is especially low, in comparison to the experimental one and to the other complexes. If the rotational correlation function obeys the Debye theory, where τ_R depends only on the volume of the complex and on the water viscosity, the values of τ_R for the $DO3A^{3-}$ and the $DOTA^{4-}$ complexes should be close to each other, which is not the case in our simulation. As will be shown at the end of this section, the simulation of the $DO3A^{3-}$ complex led to an anisotropic diffusion of the solute. This means that the solution feels a flow. This could influence the value of τ_R for $[Gd(DO3A)(H_2O)_2]$, although it seems to be essentially a translational effect more than a rotational one. Consequently we should trust the value calculated for the $DO3A^{3-}$ complex less than those calculated for the three other systems.

Another observation is that the calculated τ_R is always lower than the corresponding experimental fitted value. This can be explained by the systematic errors in the experimental values introduced by the use of single τ_R value for the various spectroscopic data. Although the effect of this drastic hypothesis should decrease the value of τ_R instead of increasing it, a compensation on the value of the ^{17}O quadropolar coupling constant might occur with this assumption, as shown by Dunand et al.[34] Another explanation can be found in a reference τ_R(water) that has been calculated for the water molecules for the various simulation (Table 4). The calculated values are always lower than the experimental value of about 2.3 ps for pure water at 300 K,[35] a result pointing out that in our simulations the rotational diffusion is slightly accelerated.

Nevertheless, the τ_R(Gd–HW)/τ_R(Gd–OW) and τ_R(Gd–HW)/τ_R(polyhedron) ratios obtained from our simulations are consistent and can be considered as close to reality, even if the absolute values of τ_R are maybe too low. The τ_R(Gd–HW)/τ_R(Gd–OW) ratio has a value of around 0.8 for cyclic complexes and around 0.7 for acyclic complexes. This difference seems reasonable since the water molecule has more degrees of freedom in a less rigid complex like the acyclic $DTPA^{5-}$ or $EGTA^{4-}$ complexes than in the very rigid $DOTA^{4-}$ and $DO3A^{3-}$ complexes. Dunand et al. obtained values for the $DOTA^{4-}$ complex of 0.65 ± 0.3. For the various complexes, the difference between τ_R(polyhedron) and τ_R(Gd–OW) is small, due to the high rigidity of the coordination polyhedron, so the two characteristic times should not be differentiated. This confirms the observation from a previous study on the $EGTA^{4-}$ complex[25] that two different τ_R values should be considered in the global NMR/EPR data analysis, one τ_R that describes the tumbling of the coordination polyhedron, including the inner-sphere water molecule(s) and a second τ_R describing the tumbling of the Gd–HW vectors. The water proton relaxivity, whose increase is a major goal in the development of MRI contrast agents, is related to τ_R(Gd–HW). A higher rigidity of the inner sphere, as in the macrocylic complexes, is a favourable contribution to a higher relaxivity.

The translational diffusion coefficient (D) can be derived from the Stokes–Einstein equation, $D = k_B T/(6\pi\eta r)$ where k_B is the Bolzmann constant, η is the viscosity of water (8.91×10^{-4} N s m^{-2} at 298 K) and r is the radius of the particle. Estimating the average radius r that describes a sphere occupying a volume equal to the Connolly molecular volumes of the complexes, we obtained $4.50 < r < 4.66$ Å, which leads to $D = (5.3\text{–}5.4) \times 10^{-10}$ m^2 s^{-1} for the various Gd^{3+} complexes. The D coefficient for $[Gd(DOTA)(H_2O)]^-$ has been measured.[36] The value obtained by Comblin et al., $D = 3.7 \times 10^{-10}$ m^2 s^{-1}, is close to the value predicted by Stokes–Einstein. The D coefficient can also be calculated from the simulations trajectories by using the Einstein–Schmoluchowski equation, $D = d^2/(6\tau)$ with d the average distance between the Gd^{3+} ion at times t and $t+\tau$, for all possible values of t. We obtained D values of 4.2, 8.9 and 9.7×10^{-10} m^2 s^{-1} for the Gd^{3+} complexes of $DOTA^{4-}$, $DTPA^{5-}$ and $EGTA^{4-}$, respectively. It was not possible to obtain a value for the $DO3A^{3-}$ complex since its trajectory was not isotropic during the 1 ns MD simulation. The D values obtained from the simulations for both acyclic complexes of $DTPA^{5-}$ and $EGTA^{4-}$ are found to be nearly twice the one obtained for the $DOTA^{4-}$ complex. The difference between the simple Stokes–Einstein and simulated values require experimental investigation by, for example, diffusion NMR measurements, as was done for the $DOTA^{4-}$ complex. In fact, for this complex where a comparison is possible, the simulated D coefficient is in very good agreement with the experimental value.

Solid angles and water exchange rate: The solid angle centred on the Gd^{3+} ion and bordered by the coordinated atoms surrounding the inner-sphere water molecule, ψ, is a possible descriptor of the steric repulsion of the complex on the water molecule.[25] Since the activation mechanism for the water exchange on Gd^{3+} polyaminocarboxylate complexes, with monoaqua nonacoordinated Gd^{3+}, is dissociative,[10] the increased steric constraint of the ligand on the inner-sphere water molecule should accelerate the water ex-

© 2003 Wiley-VCH Verlag GmbH & Co. KGaA, Weinheim

change rate. Time-averaged solid angles calculated from MD simulations are presented in Table 5. We performed a classical MD simulation of the $[Gd(TETA)]^-$ complex (TETA = 1,4,8,11-tetraazacyclotetradecane *N,N′,N″,N‴*-tetraacetic acid), where there is not enough space for an inner-sphere water molecule, in order to compare the obtained solid angle centred on the Gd^{3+} ion and bordered by the four carboxylate bound oxygen atoms (OB) to the solid angles of the other complexes. Figure 6 presents the angular projections of the inner-sphere water oxygen atom and its neighbouring coordination sites for the various complexes. The shape described by the atoms around the water molecule for $[Gd(DOTA)(H_2O)]^-$ and $[Gd(DO3A)(H_2O)_2]$(a) (centred on OWA, see Scheme 1) is close to a square. The shape around $[Gd(DO3A)(H_2O)_2]$(b) (centred on OWB) is close to a pentagon, and ψ is significantly larger (4.37 steradian, see Table 5) than for $[Gd(DO3A)(H_2O)_2]$(a) (3.33 steradian). This result leads to the following remark: If the area around the axial water is smaller than the area around the equatorial water, the water exchange rate of the axial water should be higher than the equatorial one. This is consistent with the MD simulation time-averaged distances, where the distance GD–OWA (2.61 Å) is significantly longer than GD–OWB (2.55 Å). A temperature-dependant UV/Vis spectrophotometric study of $[Eu(DO3A)(H_2O)_q]$ showed an equilibrium between $q=1$ and $q=2$.[20] At room temperature, which is also the simulation temperature, there is seven times more of the $q=2$ species than the $q=1$ species. During the whole 1 ns MD simulation the complex remains in the $q=2$ species.

Table 5. Time-averaged solid angles calculated from MD simulations on various Gd^{3+} complexes.

Complex	Solid angle [steradian]	k_{ex}[a] [10^6 s^{-1}]
$[Gd(EGTA)(H_2O)]^-$	3.60 ± 0.18	31[25]
$[Gd(DTPA)(H_2O)]^{2-}$	3.47 ± 0.15	3.3[10]
$[Gd(DOTA)(H_2O)]^-$	3.42 ± 0.16	4.1[10]
$[Gd(DO3A)(H_2O)_2]$(a)[b]	3.33 ± 0.14	6.25[20]
$[Gd(DO3A)(H_2O)_2]$(b)[b]	4.37 ± 0.14	
$[Gd(TETA)]^-$	1.97 ± 0.14	

[a] k_{ex} = the water exchange rate. [b] (a) and (b) = the solid angles around the water molecules OWA and OWB, respectively (see Scheme 1).

The shapes of the neighbouring coordination sites of the $DTPA^{5-}$ and $EGTA^{4-}$ complexes are not squares. Since these shapes also affect the steric constraint on the water molecule, it is not sufficient just to compare the values of the solid angles. An oblong shape with the same solid angle as an equilateral shape may result in a higher steric constraint. The values of solid angles for the hydrated faces of the $DTPA^{5-}$ and $EGTA^{4-}$ complexes are greater than for

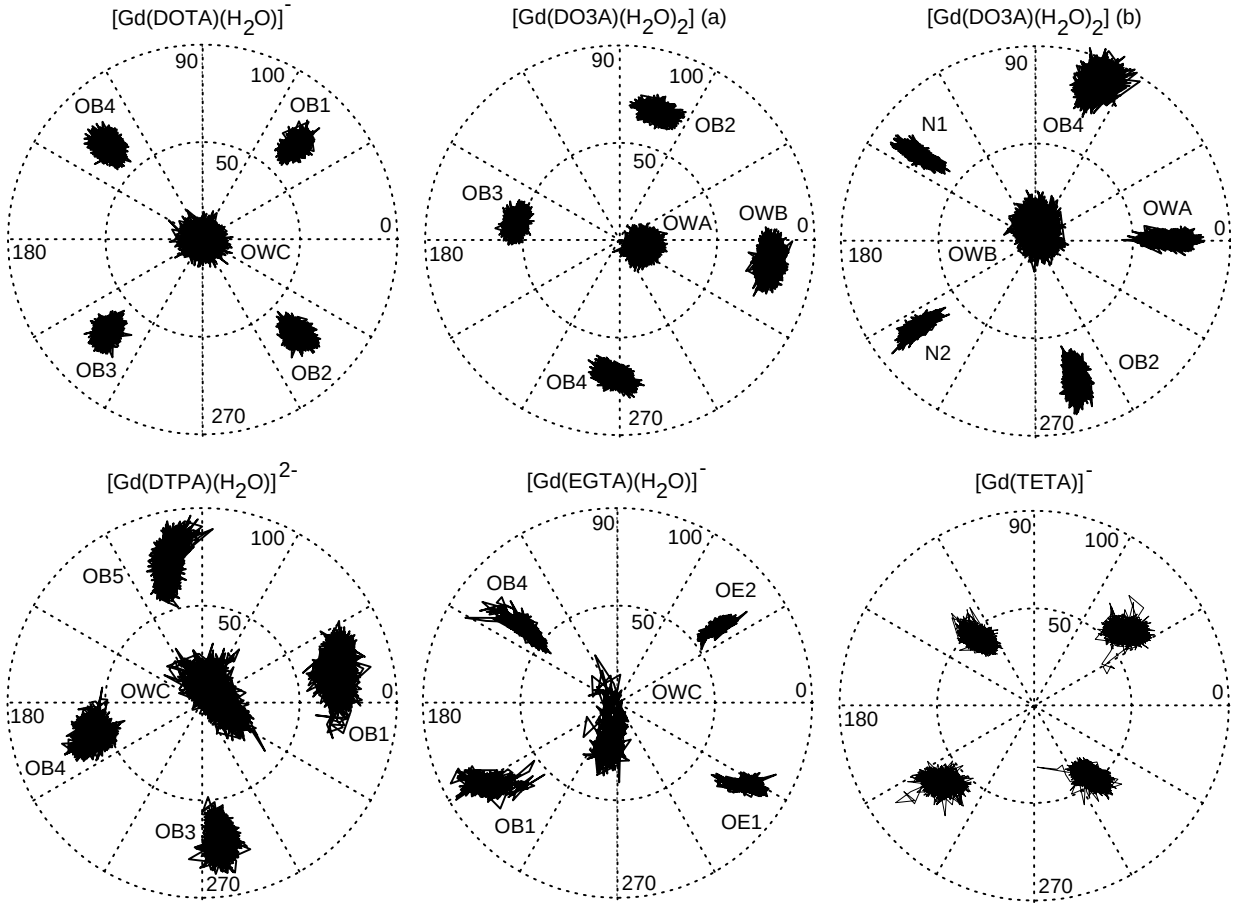

Figure 6. Angular projections of the hydrated faces of the various complexes. Atom labels are as defined in Scheme 1. $[Gd(DO3A)(H_2O)_2]$(a) depicts the projection centred over the axial water molecule OWA. $[Gd(DO3A)(H_2O)_2]$(b) shows the projection centred over the equatorial water molecule OWB.

 © 2003 Wiley-VCH Verlag GmbH & Co. KGaA, Weinheim

the $DOTA^{4-}$ complex. This is consistent for the $DTPA^{5-}$ complex, where $k_{ex}([Gd(DTPA)(H_2O)]^{2-}) < k_{ex}([Gd(DOTA)(H_2O)]^{-})$, but not for the $EGTA^{4-}$ complex, whose k_{ex} value is higher than that of the $DOTA^{4-}$ complex. This might be due to the shape of the coordination sites neighbouring the water molecule in $[Gd(EGTA)(H_2O)]^{-}$; this is the most oblong shape (Figure 6). Thus, the value of the solid angle ψ combined with the shape is a possible descriptor of the steric constraint of the complex on the inner-sphere water molecule. Consequently the solid-angle value for a faster water exchange rate should be somewhere between 2 ($[Gd(TETA)]^{-}$, $q=0$) and 3.3. A value of 2 is too small because there is no space for a water molecule. This should be taken into consideration for the design of new potential MRI contrast agents.

Conclusion

We present classical MD simulations with a force field adapted to the family of Gd^{3+} polyaminocarboxylate complexes. This has been successfully applied to two macrocyclic and two acyclic complexes, with the modelling of their internal motions and their hydration.

Fast conformational changes of the acyclic complexes of $DTPA^{5-}$ and $EGTA^{4-}$ have been observed, whereas the macrocyclic complexes of $DOTA^{4-}$and $DO3A^{3-}$ stayed highly rigid during the 1 ns simulations with only small oscillations around the initial solid-state structures. These fast conformational changes might weaken the hydration of the second water shell (longer distances and smaller hydration number), as a comparison with a previous rigid force field seems to show. This suggests that high internal mobility of the complexes disfavours the outer-sphere relaxivity.

Recently, Rast et al. have shown that the electron spin relaxation is governed by a static and a transient zero field splitting (ZFS) contribution. The static contribution depends on the coordination polyhedron geometry and its rotational correlation time. The transient contribution is a function of the magnitude of the geometry fluctuations and τ_V, the associated time constant. These fluctuations might be related to the geometrical changes of the coordination polyhedron observed in the acyclic complexes, which occur on the picosecond timescale. In the $DTPA^{5-}$ complex, the coordination polyhedron can be seen either as a distorted tricapped trigonal prism (TTP) or as three different distorted monocapped square antiprisms (MSA) in line with the three C_2 axes of the TTP. We identify three different geometrical sets that exchange with each other through the TTP intermediate. The high rigidity of the macrocyclic complexes of $DOTA^{4-}$ and $DO3A^{3-}$ did not lead to changes in the symmetry of their MSA coordination polyhedron in 1 ns. Hence we tentatively suggest that small vibrational oscillations around the idealised MSA, which typically occur on a subpicosecond timescale, might be one physical mechanism that participates in the electronic relaxation of the macrocyclic complexes. For the studied complexes the transient ZFS electron spin relaxation is faster and weaker in amplitude for the rigid macroscopic than for the stereolabile acyclic chelates.

The internal motion of the first-shell water molecule can be quantified through the ratio $\tau_R(GD–HW)/\tau_R(GD–OW)$ and is roughly constant at about 0.7 for $DTPA^{5-}$ and $EGTA^{4-}$ and 0.8 for $DOTA^{4-}$ and $DO3A^{3-}$ complexes. The high ratio of the macrocyclic complexes, which is favourable for a higher relaxivity, can be related to their rigidity.

The water exchange rate is accelerated by the steric constraint of the ligand on the exchanging water molecule for all the studied complexes. Experimentally determined water exchange rates increase with a decreasing solid angle ψ, limited by the neighbouring coordination sites of the inner-sphere water oxygen atom and centred on the Gd^{3+} ion. We estimate that $2 \lessapprox \psi < 3.3$ is a range where the water exchange rate should be the maximal possible. At $\psi \leqq 2$ there is not enough space for a water molecule in the inner sphere.

This new force field yields reasonable structural and dynamic information about the polyaminocarboxylate complexes of Gd^{III} in aqueous solution. We are confident that the method will be portable enough to allow the simulation of ligand architectures other than only the acyclic-based and the cyclen-based ones. Now that the method has proved its efficiency on well-known complexes, it can be used, as proved by a very recent paper,[37] in parallel with synthetic or analytical studies to target the design of new potential medical MRI contrast agents more efficiently.

Computational Methods

All molecular dynamics simulations were performed on an SGI Origin 200 machine with the program AMBER 6.0.[38] The methodology used to simulate the complexes $[Gd(DOTA)(H_2O)]^{-}$, $[Gd(DO3A)(H_2O)_2]$ and $[Gd(DTPA)(H_2O)]^{2-}$, as well as the choice for a force field or the atomic charge calculations, is the same as for $[Gd(EGTA)(H_2O)]^{-}$, which is described in detail elsewhere.[25] Initial molecular structures of the simulations are the published crystallographic ones,[25,39,40] except for $[Gd(DO3A)(H_2O)_2]$. In this latter case, in the solid-state the Gd^{3+} ion is complexed by the four nitrogen atoms and three carboxylate oxygen atoms of the $DO3A^{3-}$ and by two donor oxygen atoms from a carbonate counterion. The latter were replaced by two water molecules. For this complex a classical mechanics AMBER force field[41] minimisation was applied to obtain the MD starting structure. The minimised starting structure is very close to the solid state (see Supporting Information). Simulation parameters are summarised in Table 6. Atomic charges are obtained from ab initio calculations by using the program Gaussian 98[42] and are averaged by atomic type (Table 7). The charge on the Gd^{3+} ion was fixed at $+3.0$ in order to reproduce the experimental coordination number of 9 for the metal, as was done for $[Gd(EGTA)(H_2O)]^{-}$.[25] The electric dipole of the inner-sphere water molecule was adjusted to get a long lifetime for the inner-sphere water compared to the 1 ns simulation time.

Table 6. Overview of the simulation parameters[a] for the Gd^{3+} complexes of $DOTA^{4-}$, $DO3A^{3-}$, $DTPA^{5-}$ and $EGTA^{4-}$.

	Ligand			
	$DOTA^{4-}$	$DO3A^{3-}$	$DTPA^{5-}$	$EGTA^{4-}$[b]
starting structure	ref. [39]	ref. [39]	ref. [40]	ref. [25]
hydration number (q) of Gd^{3+}	1	2	1	1
no. of water molecules	815	722	1249	1364
average density [$g^{-1}cm^{-3}$]	1.056	1.042	1.058	1.038

[a] Equilibration time: 30 ps. Simulation time: 1000 ps. Stored configurations: 5000. Pressure: 1 bar. Temperature: 300 K. [b] Ref. [25].

© 2003 Wiley-VCH Verlag GmbH & Co. KGaA, Weinheim

Table 7. Averaged atomic charges calculated for the X-ray crystal structures of the Gd^{3+} complexes of $DOTA^{4-}$, $DO3A^{3-}$, $DTPA^{5-}$ and $EGTA^{4-}$.

Atom	Type	$DOTA^{4-}$	$DO3A^{3-}$	$DTPA^{5-}$	$EGTA^{4-}$[25]
GD	Gd	+3.000	+3.000	+3.000	+3.000
OB	O carboxylate (bound)	−0.943	−0.891	−0.832	−0.944
OF	O carboxylate (free)	−0.721	−0.658	−0.718	−0.718
CO	C carboxylate	+0.980	+0.838	+0.848	+0.820
CN	C methylene	−0.091	−0.116	−0.336	−0.056
HN	H methylene	+0.169	+0.152	+0.146	+0.138
N	N tertiary amine	−0.833	−0.786	−0.832	−0.944
NH	N secondary amine	–	−0.806	–	–
HN	H amine	–	+0.342	–	–
C	C N–ethylene bridge	+0.110	−0.027	+0.032	−0.016
H	H N–ethylene bridge	+0.011	+0.100	+0.138	+0.138
C	C O–ethylene bridge	–	–	–	+0.118
H	H O–ethylene bridge	–	–	–	+0.152
OE	O ether	–	–	–	−0.908
CE	C ether–ethylene bridge	–	–	–	+0.098
HE	H ether–ethylene bridge	–	–	–	+0.155
OWC	O inner-sphere water	−1.050	−1.050[a]	−1.050	−1.050
HWC	H inner-sphere water	+0.525	+0.525[a]	+0.525	+0.525

[a] The $DO3A^{3-}$ complex has two inner-sphere water molecules A and B. Here the letter C (OWC, HWC) is used as an averaged value between A and B.

For the four complexes, the optimal charges were all the same: −1.05 and +0.525 for the OW and HW, respectively. Initial molecular structures were placed into a water bath of the TIP3P water model.[43] K^+ counter ions were added at 18 Å from the Gd^{3+} center to warrant a global neutral charge. The size of the boxes was adapted to include the complex plus the counter ions. Simulation trajectory files were analysed with the KERUBIN program[44] to calculate radial distribution functions, distances and dihedral angles. Solid angles, rotational correlation times and internal basis cartesian/polar coordinates were calculated by using a custom program running in the Matlab[45] environment. All plots, statistical properties measures and least-square calculations were carried out with the program VISUALISEUR running in the Matlab environment.[46]

Acknowledgement

We thank Gaëlle Nicolle for fruitful scientific discussion and are appreciative of the Swiss National Science Foundation and the Office for Education and Science (OFES) for their financial support. This research was carried out under the EC COST Action D-18 Lanthanide Chemistry for Diagnosis and Therapy.

[1] *The Chemistry of Contrast Agents in Medical Magnetic Resonance Imaging* (Eds.: A. E. Merbach, E. Toth), John Wiley & Sons, Chichester, UK, **2001**.
[2] P. Caravan, J. J. Ellison, T. J. McMurry, R. B. Lauffer, *Chem. Rev.* **1999**, *99*, 2293–2352.
[3] R. B. Lauffer, *Chem. Rev.* **1987**, *87*, 901–927.
[4] M. T. Beck, I. Nagypàl, *Chemistry of Complex Equilibria*, Ellis Horwood, Chichester, UK, **1990**.
[5] L. Sarka, L. Burai, R. Kirali, R. Zekany, E. Brücher, *J. Inorg. Biochem.* **2002**, *91*, 320–326.
[6] E. C. Wiener, M. W. Brechbiel, H. Brothers, R. L. Magi, O. A. Gansow, D. A. Tomalia, P. C. Lauterbur, *Magn. Reson. Med.* **1994**, *31*, 1–8.
[7] D. M. J. Doble, M. Botta, J. Wang, S. Aime, A. Barge, K. N. Raymond, *J. Am. Chem. Soc.* **2001**, *123*, 10758.
[8] S. Laus, R. Ruloff, E. Toth, A. E. Merbach, *Chem. Eur. J.* **2003**, *9*, 3555–3566.
[9] R. Ruloff, E. Toth, R. Scopelliti, R. Tripier, H. Handel, A. E. Merbach, *Chem. Commun.* **2002**, *22*, 2630–2631.
[10] D. H. Powell, O. M. Ni Dhubhghaill, D. Pubanz, L. Helm, Y. S. Lebedev, W. Schlaepfer, A. E. Merbach, *J. Am. Chem. Soc.* **1996**, *118*, 9333–9346.
[11] S. Rast, P. H. Fries, E. Belorizky, *J. Chim. Phys. Phys.-Chim. Biol.* **1999**, *96*, 1543–1550.
[12] S. Rast, P. H. Fries, E. Belorizky, *J. Chem. Phys.* **2000**, *113*, 8724–8735.
[13] S. Rast, A. Borel, L. Helm, E. Belorizky, P. H. Fries, A. E. Merbach, *J. Am. Chem. Soc.* **2001**, *123*, 2637–2644.
[14] A. Borel, F. Yerly, L. Helm, A. E. Merbach, *J. Am. Chem. Soc.* **2002**, *124*, 2042–2048.
[15] W. D. Kim, G. E. Kiefer, J. Huskens, A. D. Sherry, *Inorg. Chem.* **1997**, *36*, 4128–4134.
[16] S. Aime, M. Botta, M. Fasano, M. P. M. Marques, C. F. G. C. Geraldes, D. Pubanz, A. E. Merbach, *Inorg. Chem.* **1997**, *36*, 2059–2068.
[17] R. S. Ranganathan, R. K. Pillai, N. Raju, H. Fan, H. Nguyen, M. F. Tweedle, J. F. Desreux, V. Jacques, *Inorg. Chem.* **2002**, *65*, 515–520.
[18] S. T. Frey, W. De, W. Horrocks, *Inorg. Chim. Acta* **1995**, *229*, 383–390.
[19] F. Yerly, F. A. Dunand, É. Tóth, A. Figueirinha, Z. Kovács, A. D. Sherry, C. F. G. C. Geraldes, A. E. Merbach, *Eur. J. Inorg. Chem.* **2000**, 1001–1006.
[20] E. Toth, O. M. Ni Dhubhghaill, G. Besson, L. Helm, A. E. Merbach, *Magn. Reson. Chem.* **1999**, *37*, 701–708.
[21] R. S. Dickins, S. Aime, A. S. Batsanov, A. Beeby, M. Botta, J. I. Bruce, J. A. K. Howard, C. S. Love, D. Parker, R. D. Peacock, H. Pushmann, *J. Am. Chem. Soc.* **2002**, *124*, 12697–12705.
[22] U. Cosentino, A. Villa, D. Pitea, G. Moro, V. Barone, A. Maiocchi, *J. Am. Chem. Soc.* **2002**, *124*, 4901–4909.
[23] E. S. Henriques, M. Bastos, C. F. G. C. Geraldes, M. J. Ramos, *Int. J. Quantum Chem.* **1999**, *73*, 237–248.
[24] A. Borel, L. Helm, A. E. Merbach, *Chem. Eur. J.* **2001**, *7*, 600–610.
[25] F. Yerly, K. I. Hardcastle, L. Helm, S. Aime, M. Botta, A. E. Merbach, *Chem. Eur. J.* **2002**, *8*, 1031–1039.
[26] S. Aime, M. Botta, M. Fasano, M. Paula, M. Marques, C. F. G. C. Geraldes, D. Pubanz, A. E. Merbach, *Inorg. Chem.* **1997**, *36*, 2059–2068.
[27] S. Aime, A. Barge, F. Benetollo, G. Bombieri, M. Botta, F. Uggeri, *Inorg. Chem.* **1997**, *36*, 4287–4289.
[28] S. Rast, E. Belorizky, P. H. Fries, J. P. Travers, *J. Phys Chem. B* **2001**, *105*, 1978–1983.
[29] F. A. Dunand, A. Borel, L. Helm, *Inorg. Chem. Commun.* **2002**, *5*, 811–815.
[30] D. L. Kepert, *Inorganic Stereochemistry (Inorganic chemistry concepts 6)*, Springer, Berlin, Germany, **1982**, chap. 12 and 13.
[31] H. Lammers, F. Maton, D. Pubanz, M. W. van Laren, H. van Bekkum, A. E. Merbach, R. N. Müller, J. A. Peters, *Inorg. Chem.* **1997**, *36*, 2527–2538.
[32] S. Aime, M. Botta, S. G. Crich, G. Giovenzana, R. Pagliarin, M. Sisti, E. Terreno, *Magn. Reson. Chem.* **1998**, *36*, S200-S208.
[33] S. Aime, A. Barge, A. Borel, M. Botta, S. Chemerisov, A. E. Merbach, U. Müller, D. Pubanz, *Inorg. Chem.* **1997**, *36*, 5104–5112.
[34] F. A. Dunand, A. Borel, A. E. Merbach, *J. Am. Chem. Soc.* **2002**, *124*, 710–716.
[35] M. Holz, S. R. Heil, A. Sacco, *Phys. Chem. Chem. Phys.* **2000**, *2*, 4740–4742.
[36] V. Comblin, D. Gilsoul, M. Hermann, V. Humblet, V. Jacques, M. Mesbahi, C. Sauvage, J. F. Desreux, *Coord. Chem. Rev.* **1999**, *185–186*, 451–470.

 © 2003 Wiley-VCH Verlag GmbH & Co. KGaA, Weinheim

[37] G. M. Nicolle, F. Yerly, D. Imbert, U. Bottger, J. C. Bünzli, A. E. Merbach, *Chem. Eur. J.* **2003** in press.
[38] D. A. Case, D. A. Pearlman, J. W. Caldwell, T. E. Cheatham, W. S. Ross, C. L. Simmerling, T. A. Darden, K. M. Merz, R. V. Stanton, A. L. Cheng, J. J. Vincent, M. Crowley, V. Tsui, R. J. Radmer, Y. Duan, J. Pitera, I. Massova, G. L. Seibel, U. C. Singh, P. K. Weiner, P. A. Kollman, *AMBER 6.0*, University of California, San Francisco, CA, **1999**.
[39] C. A. Chang, L. C. Francesconi, M. F. Malley, K. Kumar, J. Z. Gougoutas, M. F. Tweedle, D. W. Lee, L. J. Wilson, *Inorg. Chem.* **1993**, *32*, 3501–3508.
[40] T.-Z. Jin, S.-F. Zhao, G.-X. Xu, Y.-Z. Han, N.-C. Shi, Z.-S. Ma, H. Xuebao, *Acta Chim. Sin.* **1991**, *49*, 569–575.
[41] a) S. J. Weiner, P. A. Kollman, D. A. Case, U. C. Singh, C. Ghio, G. Alagona, S. Profeta, Jr., P. Weiner, *J. Am. Chem. Soc.* **1984**, *106*, 765; b) S. J. Weiner, P. A. Kollman, D. T. Nguyen, D. A. Case, *J. Comput. Chem.* **1986**, *7*, 230.
[42] M. J. Frisch, G. W. Trucks, H. B. Schlegel, G. E. Scuseria, M. A. Robb, J. R. Cheeseman, V. G. Zakrewski, J. A. Montgomery, R. E. Stratmann, J. C. Burant, S. Dapprich, J. M. Millam, A. D. Daniels, K. N. Kudin, M. C. Strain, O. Farkas, J. Tomasi, V. Barone, M. Cossi, R. Cammi, B. Mennucci, C. Pomelli, C. Adamo, S. Clifford, J. Ochterski, G. A. Petersson, P. Y. Ayala, Q. Cui, K. Morokuma, D. K. Malick, A. D. Rabuck, K. Raghavachari, J. B. Foresman, J. Cioslowski, J. V. Ortiz, B. B. Stefanov, G. Liu, A. Liashenko, P. Piskorz, I. Komaromi, R. Gomperts, R. L. Martin, D. J. Fox, T. Keith, M. A. Al-Laham, C. Y. Peng, A. Nanayakkara, C. Gonzalez, M. Challacombe, P. M. W. Gill, B. G. Johnson, W. Chen, M. W. Wong, J. L. Andres, M. Head-Gordon, E. S. Replogle, J. A. Pople, Gaussian 98 (Revision A.5), Gaussian, Inc., Pittsburgh, PA, **1998**.
[43] W. L. Jorgensen, J. Chandrasekhar, J. D. Madura, *J. Chem. Phys.* **1983**, *79*, 926–935.
[44] A. Porquet, KERUBIN 4.4.9, Institute of Inorganic and Analytical Chemistry, University of Lausanne, Switzerland, **2000**.
[45] Matlab 5.3.1, The Mathworks, Inc., Natick, MA, **1999**.
[46] a) F. Yerly, VISUALISEUR 2.3.4, Lausanne, Switzerland, **2002**; b) F. Yerly, OPTIMISEUR 2.3.4, Lausanne, Switzerland, **2002**.

Received: May 23, 2003 [F5175]

© 2003 Wiley-VCH Verlag GmbH & Co. KGaA, Weinheim